Acta Pharmaceutica Sinica B 2025;15(10):5444−5457

Chinese Pharmaceutical Association
Institute of Materia Medica, Chinese Academy of Medical Sciences

Acta Pharmaceutica Sinica B

www.elsevier.com/locate/apsb
www.sciencedirect.com

ORIGINAL ARTICLE

Nucleic acid-based delivery system delivering platinum drugs cooperates with siRNA for potentiated chemo-immunotherapy by reducing phosphatidylserine exposure and activating the cGAS−STING pathway

Jianqin Yan[a,*], Zijian Zhao[a], Dengshuai Wei[a], Huapeng Zheng[a], Bin He[b], Yong Sun[a,*]

[a]*Department of Pharmaceutics, School of Pharmacy, Qingdao University, Qingdao 266021, China*
[b]*National Engineering Research Center for Biomaterials, College of Biomedical Engineering, Sichuan University, Chengdu 610064, China*

Received 8 January 2025; received in revised form 16 March 2025; accepted 27 April 2025

KEY WORDS

Framework nucleic acid;
Platinum drugs;
siXkr8;
Drug delivery;
Phosphatidylserine exposure;
cGAS−STING pathway;
Immunosuppressive microenvironment;
Chemo-immunotherapy

Abstract Chemotherapeutic drugs, such as cisplatin and phenanthriplatin (PhenPt), as STING agonists to induce DNA damage and activate the cyclic GMP−AMP synthase-stimulator of interferon genes (cGAS−STING) signaling pathway provides a potential strategy for clinical chemo-immunotherapy. However, treatment with Pt-based drugs leads to irreversible ectopia of phosphatidylserine (PS), a major component of the intracellular membrane, to the surface of the cancer cells by enzymes (Xkr8). Exposed PS can bind to immune cell receptors and inhibit the presentation of tumor antigens, leading to immunosuppression and attenuation of chemotherapy. Herein, we report a novel approach to enhance chemo-immunotherapy by constructing siRNA targeted Xkr8 (siXkr8)-mediated tetrahedral framework nucleic acid nanogel structure concurrently loaded with PhenPt (siXkr8-FNG/PhenPt) for co-delivery of siRNA and Pt-based drugs. The results showed that siXkr8-FNG/PhenPt can not only be used as an efficient delivery carrier to deliver siXkr8, block the expression of Xkr8, reduce the exposure of PS on the cancer cells surface, but also act as an immune stimulant to activate cGAS−STING pathway, effectively improve the immunosuppressive microenvironment, produce antitumor immune response, and inhibit tumor growth and metastasis. Overall, this new delivery system is important for improving the effect of Pt-based drug chemotherapy, inducing immune enhancement and nucleic acid drug delivery.

*Corresponding authors.
E-mail addresses: sunyong@qdu.edu.cn (Yong Sun), yanjianqin10@163.com (Jianqin Yan).

Peer review under the responsibility of Chinese Pharmaceutical Association and Institute of Materia Medica, Chinese Academy of Medical Sciences.

https://doi.org/10.1016/j.apsb.2025.07.027

1. Introduction

Immunotherapy has shown great potential in cancer treatment[1-3]. However, the low immune response caused by limited tumor infiltrating lymphocytes (TILs) has hindered the application of immunotherapy[4,5]. Promoting effective immune stimulation of TILs is one of the important ways to maximize the efficacy of immunotherapy[3,6]. The activation of the cyclic GMP−AMP synthase-stimulator of interferon genes (cGAS−STING) signaling pathway activates a series of IFN-producing signaling cascades, stimulates antigen-presenting cells, activates antitumor T cells, initiates immune responses, and reverses the immunosuppressive microenvironment, which provides an ingenious idea for selective stimulation of TILs[7,8]. However, due to instability and low bioavailability, commonly used STING agonists are difficult to activate TILs, and easily leads to off-target, inflammation and autoimmunity, which seriously limit their application[9]. Therefore, the use of chemotherapeutic drugs as STING agonists to induce tumor cell injury and apoptosis plays a potential role in the development of clinical chemo-immunotherapy[4].

Phenanthriplatin (PhenPt) is a kind of cationic monofunctional platinum (II) drugs with steric hindrance phenanthrene ligand[10,11]. Compared with traditional platinum drugs (*e.g.*, cisplatin, carboplatin, oxaliplatin), it rapidly binds to the N7 adenosine base of DNA through covalent bonds, resulting in a unique cellular response and higher potency, leading to more severe DNA damage of tumor cells[12,13]. Yu's research group proved that PhenPt can activate cGAS−STING pathway, transform "cold tumor" into "hot tumor", realize chemical-immune synergistic therapy of tumor, and induce antitumor immunity, which has a good prospect of clinical application[12]. It is worth to note that platinum drugs and other chemotherapy drugs have weak immune effects and are prone to tumor recurrence after treatment. One of the main reasons for this is that chemotherapy can cause phosphatidylserine (PS), the main component of the cell membrane, to be irreversibly exposed to the surface of cancer cells by the flip promoting enzyme (Xkr8)[14]. PS is usually distributed on the inside of the cell membrane, but PS, which is exposed to the cell surface by Xkr8, binds to the immune cell receptor, resulting in immunosuppression, inefficacy of chemotherapy, and even tumor recurrence[15,16]. Therefore, blocking Xkr8 expression can prevent PS from flipping to the surface of cancer cells, substantially improve the immune microenvironment, and effectively inhibit tumor growth. Unfortunately, but so far, there is no inhibitor to block the expression of Xkr8, so blocking its expression through small interference RNA (siXkr8) is an effective way to induce platinum-based chemo-immunotherapy enhancement[17].

Unfortunately, due to its anionic properties, siRNA cannot cross the cell membrane, and its poor physiological stability, easy removal by nucleases in serum, and short half-life seriously hinder the clinical application and development of RNA interference (RNAi) technology[18,19]. Great advances have been made in viral or non-viral vectors for siRNA delivery, but significant challenges remain such as mutagenicity, transfection efficiency and safety issues. Micelles and liposomes composed of cationic polymers and lipids are the most commonly used non-viral vectors that can efficiently compress siRNA and deliver it to target cells by electrostatic action. However, the effect of gene silencing is closely related to the cationic nature of the carrier. The higher the cationic charge of the carrier, the more effectively it can compress the siRNA and effectively silence the expression of the target gene, but the toxicity of the cationic material is enhanced at this time, which will produce serious side effects. In addition, cationic nanoparticles interact strongly with negatively charged proteins in plasma, resulting in instability of nanocarriers and rapid clearance during circulation, reducing the therapeutic efficacy of RNAi.

In recent years, a variety of DNA nanostructures, such as spherical nucleic acids[20,21] and framework nucleic acids (FNA)[22], have been developed for nucleic acid delivery. Unlike cationic carriers, which rely on electrostatic interactions, negatively charged DNA nanostructures rely on covalent binding or molecular recognition to compress functional nucleic acids and form delivery complexes[23,24]. Embedding siRNA into DNA nanostructures has become a new strategy for siRNA delivery. The DNA structure provides a protective barrier for better stability and gene silencing effect of siRNA, and avoids the potential cytotoxicity of cationic carriers, with higher biosafety and lower immunogenicity.

Based on this, we proposed to construct siXkr8-mediated FNA nanogel structure (siXkr8-FNA nanogel, siXkr8-FNG) with FNA as the backbone structure and siXkr8 as the cross-linking chain. PhenPt, a platinum drug with a concomitant aromatic cyclic structure, was encapsulated into an FNA nanogel structure (siXkr8-FNG/PhenPt) *via* intercalation and electrostatic interactions to achieve co-delivery of siXkr8 and Pt-based drugs (Scheme 1). The construction of FNA nanogel formed a protective barrier for the internally loaded siRNA, which effectively safeguarded the physiological stability and structural integrity of siXkr8 and ensured its pharmacodynamic properties. siXkr8-mediated construction of FNA nanogel broke the mode of cationic carrier delivery, realizing a new strategy for siRNA delivery. Meanwhile, the loading of FNA nanogel reduced the toxicity of the cationic drug PhenPt and enables the activation of the cGAS−STING pathway while chemotherapy was administered. It is also assisted by the role of siXkr8 in indirectly regulating the distribution of PS on the plasma membrane, which solved the problems of weak immune effect and tumor recurrence after Pt-based drugs. Hence, the strategy of siRNA-mediated drug-loaded FNA nanogel combined to reduce PS exposure and activate the cGAS−STING pathway brings great potential for enhancing chemo-immunotherapy.

2. Materials and method

2.1. Materials

All DNA oligonucleotides and siRNA were purchased from Sangon Biotech Co., Ltd. (Shanghai, China). Cispaltin, $AgNO_3$ and phenanthridine were purchased from Sigma—Aldrich Co.

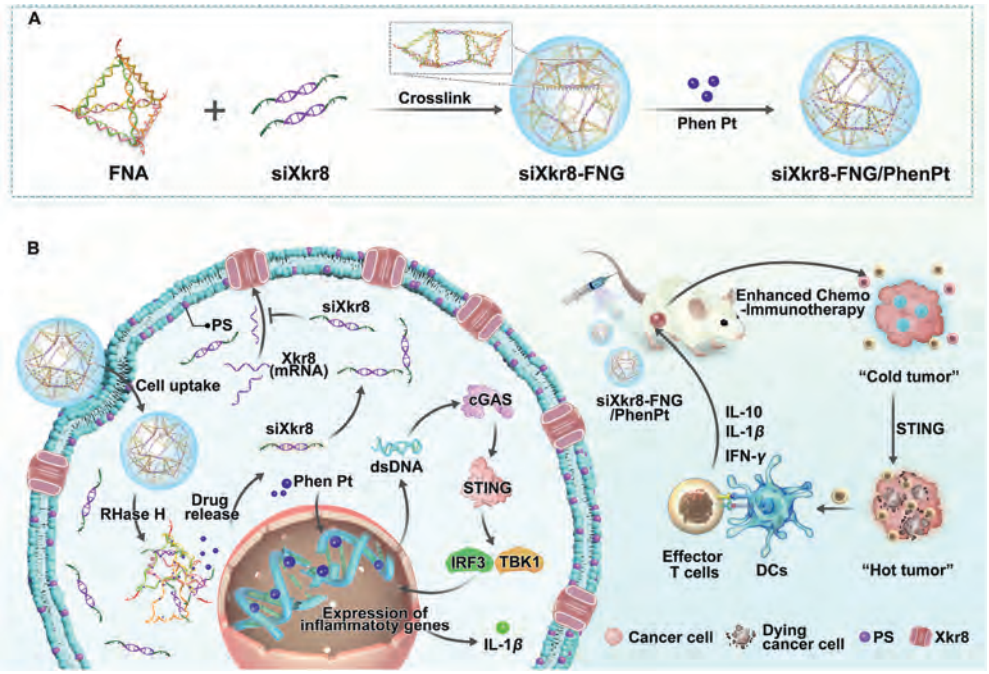

Scheme 1 Diagram of synthetic procedures and antitumor mechanisms of siXkr8-FNG/PhenPt. (A) Illustrations of synthetic procedures of siXkr8-FNG/PhenPt. (B) Schematic illustration of siRNA-mediated tetrahedral framework nucleic acid nanogel reduces phosphatidylserine exposure and activates the cGAS−STING pathway for potentiated chemo-immunotherapy.

(Steinheim, Germany). GelRed stain solution was purchased from Biotium (CA, USA). Green fluorescent protein (GFP) antibody, 4′,6-diamidino-2-phenylindole (DAPI) and Lyso-tracker green were purchased from Beyotime Institute of Biotechnology (Nanjing, China). ELISA kits were acquired from Dakewei Biotech Co., Ltd. (Shenzhen, China). All other reagents were of analytical grade and purified before use.

2.2. *Synthesis of phenanthriplatin (PhenPt)*

Cisplatin and $AgNO_3$ were dissolved in DMF (30 mL) and stirred at 55 °C for 16 h in the dark. After the solution turned into a light gray cloudy liquid, phenanthridine (153 mg, 0.9 mmol) was dissolved in the above filtered solution and continued to stir in the dark. And DMF was removed after 16 h by rotary evaporation. Subsequently, methanol was added to dissolve and filter to remove the precipitation. Finally, anhydrous ether was added and the precipitation was collected. The precipitation was washed with methanol and ether, dried and collected, and the resulting fixed powder was Phenanthriplatin (abbreviations: PhenPt (II), PhenPt).

2.3. *Synthesis and characterizations of siXkr8-FNG*

The FNA were synthesized as previously reported[22,25]. The oligonucleotides with equal molar amount (S1, S2, S3, S4 or S1-T, S2-T, S3-T, S4-T) were mixed in TM buffer (20 mmol/L Tris base, 5 mmol/L $MgCl_2$, pH = 8.0, final concentration: 2 μmol/L). The solution was heated at 95 °C for 15 min and then quickly transferred to 4 °C for cooling. The characterizations of FNA were verified by gel electrophoresis, dynamic light scattering (DLS, Zeta sizer Nano ZS, Malvern Instruments, Malvern, UK) and transmission electron microscopy (TEM, HT7700, Hitachi, Japan). To obtain the sticky-end siRNA linker, the sense siXkr8 and antisense siXkr8 dissolved in DEPC water were mixed at equimolar ratio and putted in the reverse recording PCR instrument for gradient annealing to room temperature to obtain successfully assembled siRNA. The siRNA of GFP or scramble linker was prepared as described above, and the prepared siRNA was stored at −20 °C.

siXkr8-FNG was prepared by molecular recognition between bases. In brief, FNA (2 μmol/L) and siRNA (4 μmol/L) with different molar ratios (FNA: siRNA = 1:1.2, 1:1.4, 1:1.6, 1:1.8, 1:2, 1:2.2, 1:2.4) were mixed and shacked at 37 °C to obtain siXkr8-FNG. The product was verified by agarose gel electrophoresis analysis.

The size change of siXkr8-FNG or siXkr8-FNG/PhenPt in phosphate buffer saline (PBS) and 10% serum under different time was detected by DLS. TEM was used to characterize the morphology of siXkr8-FNG.

In addition, FNG with FAM-labeled siXkr8 was prepared and incubated in different media (pH 7.4 and 5.0). And pH 5.0 buffer with 200 U/mL RNase H was set to simulate the intracellular environment. The release of siXkr8 was detected by microplate reader (BioTek Synergy H4).

2.4. *Preparation and characterizations of siXkr8-FNG loaded PhenPt (siXkr8-FNG/PhenPt)*

SiXkr8-FNG (1 μmol/L) and PhenPt (100 μmol/L, dissolved in H_2O) were mixed and incubated at 37 °C for 6 h. The mixed solution was filtered by centrifugation (MWCO 30 kDa) and concentrated to obtain siXkr8-FNG loaded with PhenPt (siXkr8-FNG/PhenPt). The synthesis of siXkr8-FNG/PhenPt was verified by 0.5% agarose gel electrophoresis analysis.

The size and zeta potential of siXkr8-FNG and siXkr8-FNG/PhenPt were measured by DLS. Meanwhile, the change of circular

dichroism (CD) (Chirascan plus, Applied photophysics) before and after PhenPt loading was detected.

2.5. Cellular uptake

The cellular uptake was investigated using confocal laser scanning microscopy (CLSM) and flow cytometry (FCM). 4T1 cells were inoculated in glass dishes and incubated for 24 h, then incubated with siXkr8-FNG/PhenPt (FNG was modified with Cy5) at 37 °C for 1 or 4 h, respectively. After completion of incubation, the cells were washed, fixed, stained with DAPI, photographed and analyzed using CLSM. 4T1 cells were seeded in well plates for incubation and subsequently cultured with siXkr8 and siXkr8-FNG/PhenPt for 1 or 4 h, respectively. Finally, the cells were collected, and resuspended in PBS before FCM analysis.

In addition, 4T1 cells were seeded in 6-well plates and cultured for 24 h, then cisplatin, PhenPt and siXkr8-FNG/PhenPt (Pt concentration: 10 μmol/L) were added and incubated for 1 or 4 h, respectively. 4T1 cells were washed with PBS and collected, and cells were subsequently nitrified and diluted with nitric acid. The uptake of Pt and Pt content in the nucleus was measured by inductively coupled plasma mass spectrometry (ICP-MS).

2.6. Endosomal escape

The co-localization of siXkr8-FNG/PhenPt and endosome was investigated by CLSM. 4T1 cells were incubated with siXkr8-FNG/PhenPt (FNG modified with Cy5, concentration: 100 nmol/L). After 2 h, the medium was changed and the cells were cultured with fresh medium for another 0.5, 2, or 4 h. Finally, the cells were washed and fixed, stained with Lyso-Tracker Green and photographed by CLSM. Meanwhile, the Pearson correlation coefficient (PCC) between siXkr8-FNG and endosome was analyzed by Image J software to further evaluate the colocalization.

2.7. Cytotoxicity assays

First, the biocompatibility of FNA was evaluated. L929, 4T1 or MCF-10A cells were seeded in 96-well plates. After 24 h, the medium was replaced and the cells were incubated for another 24 h by adding medium containing different concentrations of FNA. After the completion of the culture, the original medium was abandoned and the culture medium containing MTT (0.5 mg/mL) was added to each well for 4 h. Then dimethyl sulfoxide (150 μL) was used to replace the above medium. The absorbance at 490 nm was measured by microplate reader and the cell viability was calculated.

The cytotoxicity of the nanoparticles was evaluated in 4T1 cells, MCF-7 cells, A549 cells and drug-resistant A549/DDP cells. In the case of 4T1 cells, the procedure was described as follows: 4T1 cells were cultured in 96-well plate for 24 h, then the medium was changed and the medium containing cispaltin, PhenPt, siXkr8-FNG/PhenPt with different concentrations of Pt was added to culture for another 24 h. After 24 h, cell viability was measured by MTT assay as described above. And the cytotoxicity of nanoparticles to MCF-7, A549 and A549/DDP cells was determined similarly to that described above.

2.8. Gene silencing and RT-qPCR assay

RAW 264.7 cells expressing GFP were co-cultured with Lipo-siGFP, siGFP-FNG, siGFP-FNG/PhenPt, siNC-FNG (scramble siRNA mediated FNG, as a negative control) (siRNA concentration: 20 nmol/L) for 12 h, respectively. Thereafter, the cells were washed and fixed, and the expression of green fluorescence was observed after DAPI staining. Furthermore, RAW 264.7 cells after different treatments were collected, washed and lysed using EBC 250 lysis buffer. After determination of protein concentration, the equal amount of protein was separated on SDS-PAGE gel, transferred, and hybridized with the primary antibody and secondary antibody in turn for Western blot (WB) analysis to determine the expression of GFP.

For RT-qPCR assay, 4T1 cells were co-cultured with Lipo-siXkr8, siXkr8-FNG, siXkr8-FNG/PhenPt, siNC-FNG/PhenPt, PhenPt and cisplatin for 12 h, respectively. Total RNA was collected after isolation using Trizol reagent (Invitrogen, USA) according to the instructions. Total RNA was reverse transcribed into cDNA using TransGen reverse transcriptase, and qPCR was performed in a CFX96 Real-time PCR system (Bio-Rad, USA). Reactions were incubated and cycled for 40 cycles. β-Actin was used as an endogenous control for standardization.

2.9. The exposure of phosphatidylserine

4T1 cells were seeded and cultured for 24 h. The medium (2 mL) containing cisplatin, PhenPt, siXkr8-FNG/PhenPt or siNC-FNG/PhenPt (Pt concentration:10 μmol/L) was added for further 24 h incubation. Cells were subsequently harvested and analyzed by FCM after staining with Annexin V-FITC and Zombie NIR.

2.10. Activation of the STING pathway

Comet Assay: the cells were treated with cisplatin, PhenPt, siXkr8-FNG or siXkr8-FNG/PhenPt for 12 h. The collected cells were mixed with low-melting agarose, then the cells were dropped onto glass slides that were adhered to normal melting agarose and lysed in lysis buffer. Electrophoresis was performed at 20 V for 20 min, and finally DNA was stained with propidium iodide to visualize the comet tail under a fluorescence microscope.

Quantification of dsDNA: after cells were treated with cisplatin, PhenPt, siXkr8-FNG, or siXkr8-FNG/PhenPt for 10 h, the medium was changed and the incubation was continued for 12 h. Subsequently, 4T1 cells supernatant was centrifuged and 2 μL sample was taken out to detect dsDNA through a NanoDrop Spectrophotometer (Thermo Fisher Scientific, USA).

4T1 cells were seeded and cultured for 24 h. The medium was removed and medium containing cisplatin, PhenPt, siXkr8-FNG or siXkr8-FNG/PhenPt was added for further 24 h. Subsequently, cells were harvested and lysed. And proteins were quantified and separated on SDS-PAGE gel, transferred and incubated separately with primary antibodies (γ-H2AX, p-STING, cGAS and p-TBK1) associated with the STING pathway. Then Western blot analysis was performed after hybridization with relevant secondary antibodies.

2.11. Biodistribution study

5-week-old female BALB/c mice were purchased from Beijing Vital River Laboratory Animal Technologies Co., Ltd. (Beijing, China). All animal experiments were approved by the Animal Care Ethics Committee of Qingdao University (Qingdao, China). Tumor models were established by subcutaneous injection of 4T1 cells on the right side of mice. The tumor volume (V) was calculated using Eq. (1):

$$V = a \times b^2/2 \quad (1)$$

where *a* represents length and *b* represents width. When the *V* reached 200 mm^3, mice were randomly divided into two groups and intravenously injected with free Cy5 or Cy5-modified siXkr8-FNG, respectively. Fluorescence images were collected at different time points by IVIS spectrum imaging system after injection. Finally, major organs and tumors were collected for *ex vivo* imaging. Pt content in major organs and tumors of mice after siXkr8-FNG/PhenPt injection (3.5 mg Pt/kg body weight) was determined by ICP-MS.

2.12. Tumor growth inhibition in vivo

When the tumor volume of mice reached ~150 mm^3, the mice were randomly divided into five groups and injected with saline, PhenPt, siXkr8-FNG, siXkr8-FNG/PhenPt or siNC-FNG/PhenPt *via* the tail vein, respectively. Mice were given the preparation every 3 days for a total of four injections. And the changes of body weight and tumor volume were also recorded and analyzed. After 18 days, the mice were sacrificed, and the major organs were stained with hemotoxin and eosin (H&E). The tumors were dissected and weighed, and stained with H&E, TUNEL and Ki-67.

2.13. In vivo antitumor immunity

Spleens or tumors from mice after different treatments were collected, ground and filtered to obtain single-cell suspensions of spleens or tumors. Cell suspensions of spleens were stained with anti-mouse CD11c, anti-mouse CD86, and anti-mouse CD80 to detect the maturation of dendritic cell. Cell suspensions of tumors were stained with anti-mouse CD3, anti-mouse CD8, anti-mouse CD4 and anti-mouse FoxP3 to detect cytotoxic T lymphocyte cells (CTL) and regulatory T cells (Tregs), respectively. In addition, the serum of the treated mice was collected and the secretion of related cytokines (such as interleukin-10 (IL-10), interleukin-1β (IL-1β), tumor necrosis factor (TNF-α) and interferon-γ (IFN-γ)) in serum was detected by ELISA. Similarly, the immunofluorescence or histochemical images of CD8 and STING of tumor tissues were observed after treatment.

2.14. Statistical analysis

Data are presented as mean ± standard deviation (mean ± SD). And data were evaluated the statistical significance using student's *t*-test or ANOVA analysis.

3. Results and discussion

3.1. Characterization of siXkr8-FNG and siXkr8-FNG/PhenPt

Both FNA and siXkr8-mediated FNG (siXkr8-FNG) in this study were synthesized. Fig. 1A shows the schematic diagram of the synthesis, and the related DNA or RNA oligos are shown in Supporting Information Table S1. FNA synthesis was performed according to previous reports[22,25,26] and confirmed by agarose gel electrophoresis. The results (Supporting Information Fig. S1A) showed that FNA migrated at a slower rate than other DNA combinations due to its larger molecular weight, proving the successful construction of FNA. DLS results show its diameter about 8.2 nm, and presents a tetrahedral structure (Fig. S1B and Fig. S1C). In addition, ultraviolet/visible (UV/vis) spectra

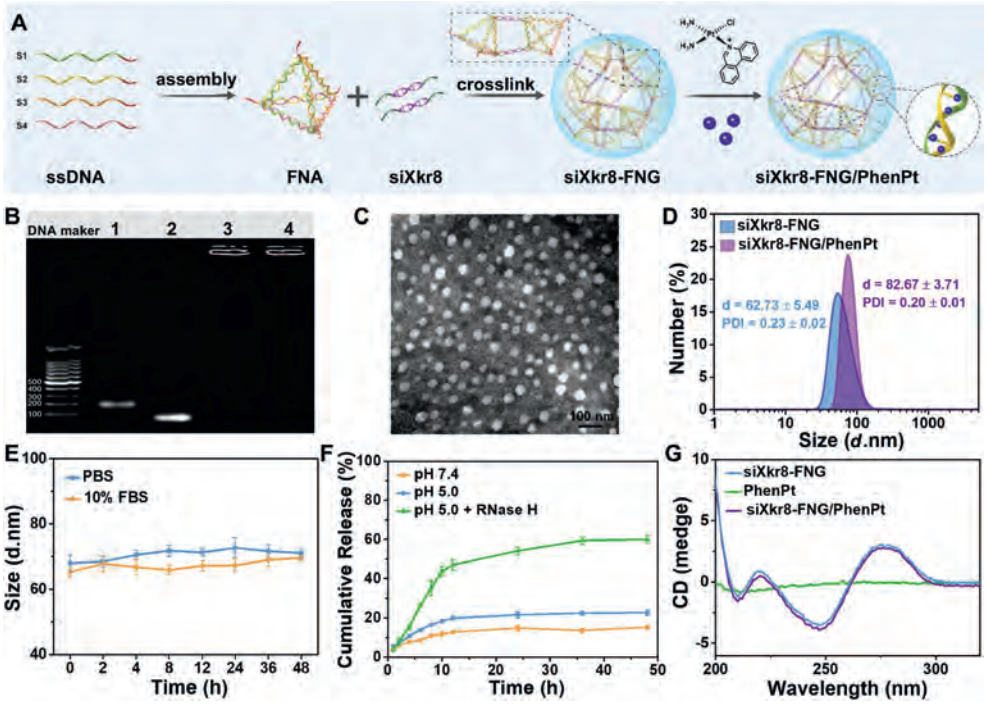

Figure 1 The characterization of siXkr8-FNG and siXkr8-FNG/PhenPt. (A) Schematic illustration of the preparation of siXkr8-FNG and siXkr8-FNG/PhenPt. (B) The results of gel electrophoresis (line 1: FNA, line 2: siXkr8, line 3: siXkr8-FNG, line 4: siXkr8-FNG/PhenPt). (C) The TEM image of siXkr8-FNG. (D) DLS results of before and after PhenPt loading with siXkr8-FNG. (E) The size changes of siXkr8-FNG in PBS and 10% FBS (n = 3, mean ± SD). (F) The drug release curves of siXkr8 from FNG in different media (n = 3, mean ± SD). (G) Circular dichroism spectra of siXkr8-FNG, PhenPt and siXkr8-FNG/PhenPt.

(Fig. S1D) showed that FNA have characteristic absorbance peaks of DNA (260 nm). Theoretically, a relatively pure nanogel can be obtained when the ratio of FNA: siRNA is 1:2. Based on this, different ratios of FNA and siXkr8 were incubated to obtain nanogel structures (FNG). Using gel electrophoresis, the assembly of FNA and siXkr8 into FNG was confirmed (Supporting Information Fig. S2A). It was found that excessive siXkr8 appeared in the lane when the ratio of FNA: siXkr8 was greater than 1:2. To better exert the protective effect of FNA on siXkr8, we chose 1.1.6 to prepare siXkr8-FNG and carried out the subsequent experimental study. Compared with FNA and siXkr8, siXkr8-FNG had a lower mobility (Fig. 1B, line 3), and the TEM image showed that siXkr8-FNG was homogeneous spherical with a uniform distribution and no obvious aggregation, and the size was about 62.73 nm as tested by DLS (Fig. 1C and D).

The stability of siXkr8-FNG was detected by DLS (Fig. 1E). There was no significant change in the particle size of siXkr8-FNG, which indicated that the particles had no obvious disassembly behavior and could be stable in PBS or 10% FBS for at least 48 h, and had good storage and serum stability. Given the weak acidity of the tumor microenvironment, siRNA release at different pH was characterized. siXkr8-FNG enters the cell *via* endocytosis and then the nanogel are exposed to various enzymes that ultimately promote RNase H-mediated release of siXkr8 from FNG[27]. Excitingly, the results in Fig. 1F clearly revealed that the release behavior of siXkr8 was closely related to pH and incubation time. Trace amounts of siXkr8 were released under normal physiological conditions, and the release rate of siXkr8 from FNG at pH 5.0 was faster than that in medium at pH 7.4. Notably, the presence of RNase H (200 U/mL) at pH 5.5 significantly facilitated the release of siXkr8, and the amount of release increased with the incubation time. The effective release of siXkr8 lays the foundation for subsequent achievement of siRNA-mediated gene silencing and amplification of platinum-based drug efficacy.

As a cationic monofunctional platinum (II) drug and a DNA binder, the antitumor mechanism of PhenPt is similar to that of classical platinum-based drugs. And its unique cellular response and higher potency lead to more severe DNA damage[12,28,29]. However, as a cationic drug, it is easily bound to plasma proteins, resulting in rapid clearance of PhenPt, poor efficacy *in vivo*, and obvious side effects, which severely limits its application. To improve the delivery and application of PhenPt, enhance the immune effects of FNA while maximizing the activation of cGAS−STING pathway[30,31], PhenPt was incorporated into DNA nanostructures to form siXkr8-FNG/PhenPt. PhenPt was synthesized following the routes of Fig. S2 and characterized by ^{1}H NMR (Supporting Information Fig. S3). Subsequently, PhenPt-loaded siXkr8-FNG was characterized by gel electrophoresis, DLS and TEM. The results showed that the migration of siXkr8-FNG did not change after PhenPt-loading (Fig. 1B, line 4). siXkr8-FNG/PhenPt were spherical without obvious aggregation (Supporting Information Fig. S4A), and the size increased to about 82.67 nm (Fig. 1D). The stability results (Fig. S4B) showed that siXkr8-FNG/PhenPt was stable in PBS, and the size fluctuation in the later period might be caused by the trace release of PhenPt. Due to the positive electropositive nature of PhenPt, the zeta potential of siXkr8-FNG changed from −14.7 to −3.1 mV after loading PhenPt (Fig. S2B). All of the above indicated the successful loading of PhenPt. Meanwhile, circular dichroism spectroscopy showed no significant change between siXkr8-FNG and siXkr8-FNG/PhenPt (Fig. 1G), indicating that the loading of PhenPt did not affect the configuration of FNG and the DNA nanostructures, also consistent with previous reports[31].

3.2. Cell uptake and cytotoxicity

The biocompatibility of nanocarriers is the primary condition for the delivery system, so the cytocompatibility of FNA to normal cells (L929 cells and MCF-10A) and tumor cells (4T1 cells) was first determined by MTT assay. The results (Supporting Information Fig. S5A) showed that the survival rate of L929, MCF-10A or 4T1 cells was more than 80%, indicating the excellent biocompatibility of FNA, which is important for drug delivery systems. Then, the efficient internalization of siXkr8-FNG/PhenPt into 4T1 cells was demonstrated subsequently by CLSM. And in this study, FNA was labeled with Cy5 to track the nanogel inside the cells. The intracellular red fluorescence (Cy5) gradually increased with incubation time, reflecting the effective internalization of siXkr8-FNG/PhenPt and its time-dependent cellular uptake (Fig. 2A). It should be noted that siXkr8-FNG/PhenPt could enter the nucleus after 4 h of incubation, which would be beneficial for the pharmacological effects of PhenPt. Next, the cellular uptake of siXkr8-FNG/PhenPt was quantified by FCM using siXkr8 as a control. No significant fluorescence intensity was found in the cells after siXkr8 linker alone incubation, even incubated for 4 h (Fig. 2C), suggesting that siXkr8 alone was virtually inaccessible to the cells because nucleic acids are known to be negatively charged molecules. The results of FCM and statistical analysis (Fig. 2C and D) proved that the uptake of siXkr8-FNG/PhenPt was positively correlated with incubation time, which was consistent with the results of CLSM analysis. In addition, the uptake of PhenPt was also quantified by inductively coupled plasma-mass spectrometry (ICP-MS) due to the presence of Pt atoms. The results (Fig. 2E) show that more Pt could be observed after 4T1 cells treated with siXkr8-FNG/PhenPt compared with free cisplatin and PhenPt. After 4 h, Pt uptake in 4T1 cells treated with siXkr8-FNG/PhenPt reached 0.506 μg Pt/million cells, which was 2.12-fold higher than that with cisplatin. To further investigate the platinum content in the nucleus, we extracted the membrane, nucleus, and cytoplasm of cancer cells treated with siXkr8-FNG/PhenPt. The results in Supporting Information Fig. S6A showed that the proportion of Pt in the nucleus to total cancer cells was positively correlated with incubation time. After 12 h, the proportion of Pt in the nucleus treated with siXkr8-FNG/PhenPt was about 48.1%. Genomic DNA was extracted from the cancer cells and identified to be Pt-DNA adducts (Fig. S6B). The results showed that the amount of Pt-DNA adducts in the genomic DNA of cells treated with siXkr8-FNG/PhenPt significantly increased. This suggested effective nuclear accumulation and the DNA adduction of Pt.

The lysosomal escape ability is very important for drug delivery systems, especially those whose drug targets are not lysosomes. Cellular lysosomes were stained with lysotracker to investigate whether lysosomal escape could be achieved after internalization of siXkr8-FNG/PhenPt, and the transport of siXkr8-FNG/PhenPt was observed by CLSM. As shown in Fig. 2B, the observed red fluorescence (FNG modified with Cy5) provided evidence that siXkr8-FNG/PhenPt was efficiently internalized in 4T1 cells by the endocytic pathway. Strong yellow fluorescence signals (overlap of red and green signals) of the internalized were co-localized with lysosomes after 0.5 h with a Pearson correlation coefficient (PCC) of 0.67. With the extension of incubation time, the yellow fluorescence in the cells gradually decreased with time, and the PCC decreased to −0.10 after 4 h,

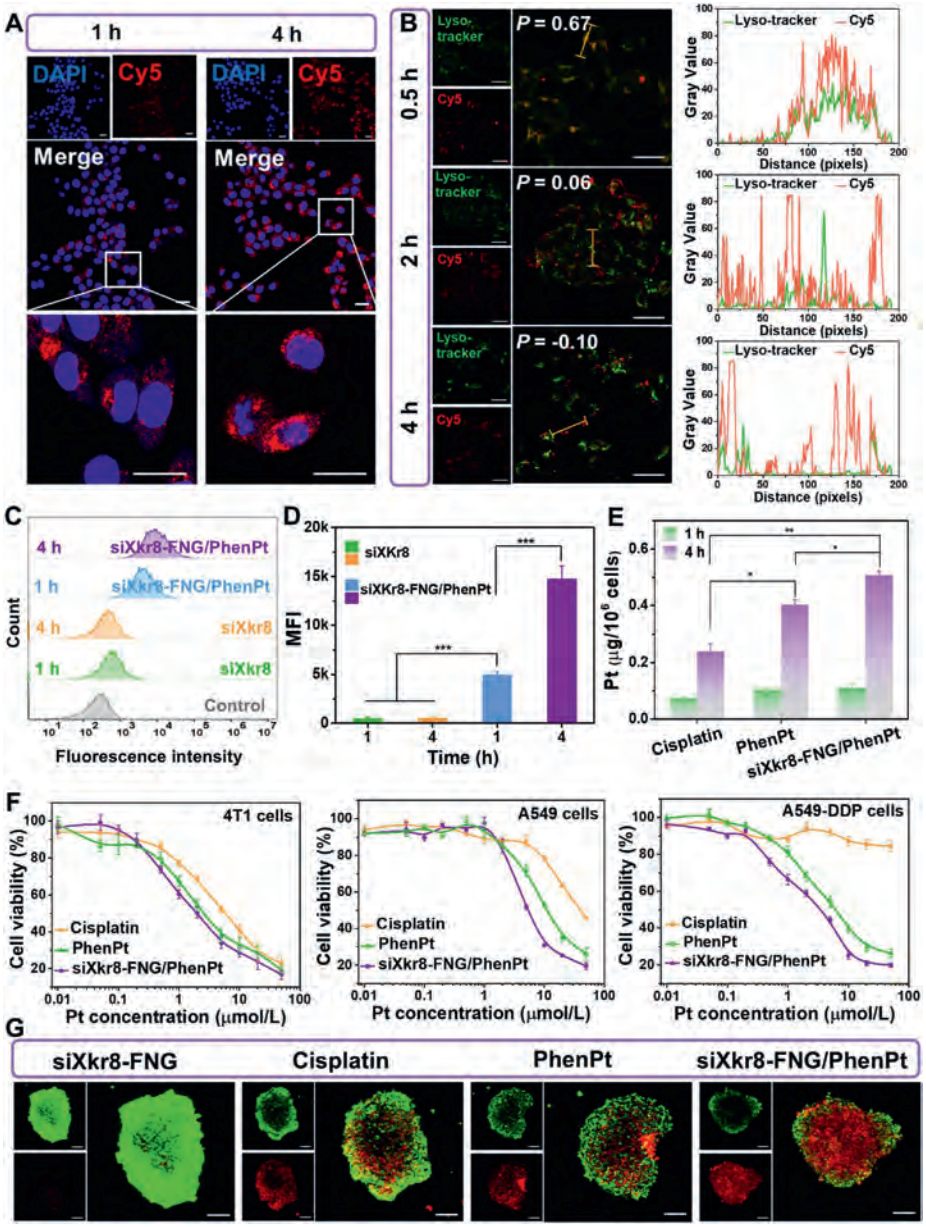

Figure 2 Cell uptake of siXkr8-FNG/PhenPt *in vitro*. (A) The CLSM images of 4T1 cells treated with siXkr8-FNG/PhenPt for 1 and 4 h (the scale bar represents 25 μm, DAPI (blue): $\lambda_{ex}/\lambda_{em}$ = 364 nm/454 nm, Cy5 (red): $\lambda_{ex}/\lambda_{em}$ = 650 nm/670 nm). (B) The CLSM images, colocalization analysis, and PCC of siXkr8-FNG/PhenPt and Lysosome (the scale bar represents 25 μm, Lyso-Tracker (green): $\lambda_{ex}/\lambda_{em}$ = 504 nm/511 nm, Cy5 (red): $\lambda_{ex}/\lambda_{em}$ = 650 nm/670 nm). (C, D) The FCM results after 4T1 cells treated with siXkr8 or siXkr8-FNG/PhenPt for different time (n = 3, mean ± SD, ***P < 0.005). (E) Intracellular Pt determination of 4T1 cells treated with cisplatin, PhenPt, and siXkr8-FNG/PhenPt (n = 3, mean ± SD, *P < 0.05, **P < 0.01). (F) The cytotoxicity of siXkr8-FNG/PhenPt against 4T1 cells, A549 cells or A549-DDP cells. (G) CLSM images of MTSs treated with siXkr8-FNG, cisplatin, PhenPt, and siXkr8-FNG/PhenPt *via* live/dead staining (the scale bar represents 50 μm, Calcein AM (green): $\lambda_{ex}/\lambda_{em}$ = 494 nm/517 nm, PI (red): $\lambda_{ex}/\lambda_{em}$ = 535 nm/617 nm).

indicating that the DNA nanostructure had successfully escaped from the lysosomes, which may stem from the cationic PhenPt-induced proton sponge effect.

To investigate the cytotoxicity of siXkr8-FNG/PhenPt, the inhibitory effects of cisplatin, PhenPt, and siXkr8-FNG/PhenPt on the proliferation of wild type (4T1, A549 and MCF-7 cells) and multidrug resistant (A549-DDP) cells were evaluated *in vitro* (Fig. 2F and Fig. S5B). Compared with cisplatin, both PhenPt and siXkr8-FNG/PhenPt showed superior inhibitory effects on tumor proliferation *in vitro*, especially in A549-DDP cells. For A549-DDP cells, the IC_{50} value of cisplatin was greater than 50 μmol/L, and the IC_{50} value of siXkr8-FNG/PhenPt was about 3.47 μmol/L. This result may be attributed to the good uptake of tetrahedral DNA nanostructures by drug-resistant cells, as well as the effective inhibition of PS exposure by siXkr8, which improved the sensitivity of tumor cells to the chemotherapeutic drug PhenPt and achieved chemotherapeutic potentiation. Multi-cellular tumor spheroids (MTSs) can mimic *in vivo* tumors with physiological

parameters, such as complex multicellular structures and multi-molecule transport barriers[26,32]. Therefore, MTSs were constructed as a 3D tumor model to assess the antitumor ability of siXkr8-FNG/PhenPt. The results (Fig. 2G) showed that siXkr8-FNG was not significantly toxic and the MTSs were mainly composed of living cells (green). In contrast, the siXkr8-FNG/PhenPt-treated MTSs appeared to have a significantly larger number of dead cells (red) than in groups cisplatin and PhenPt, which was consistent with the results of cytotoxicity test.

3.3. Gene silencing and inhibition of siRNA-mediated PS exposure

siXkr8-FNG/PhenPt could be efficiently internalized by 4T1 cells and exhibited prominent *in vitro* antitumor effects. Next, we focused on validating the gene silencing effect of siXkr8-FNG/PhenPt and the blocking effect of siXkr8-mediated PS exposure. In order to visualize the gene silencing effect, we first constructed FNG nanogels by siGFP, which can inhibit the expression of green fluorescent protein (GFP), and chose RAW 264.7 cells expressing GFP to validate the gene silencing ability of FNG. Meanwhile, Lipofectamine 2000-transfected siRNA (Lipo-siGFP) was used as a positive control, and cells treated with FNG with scrambled siRNA (siNC-FNG) were used as a negative control. As shown in Fig. 3A, all the nanoparticles or FNG loaded with siGFP effectively reduced the intensity of green fluorescence, while negligible GFP silencing was observed in the cells treated with siNC-FNG, which was consistent with the WB analysis of GFP expression (Fig. 3B and Supporting Information Fig. S7A). The above results indicate that knockdown of GFP is a sequence-specific RNAi process, and both siGFP-FNG and siGFP-FNG/PhenPt could significantly reduce the expression of GFP, confirming that siXkr8-FNG could be used as an excellent siRNA delivery vector for target gene silencing.

Blocking Xkr8 expression and the resulting PS turnover on the surface of cancer cells further enhances the efficacy of platinum-

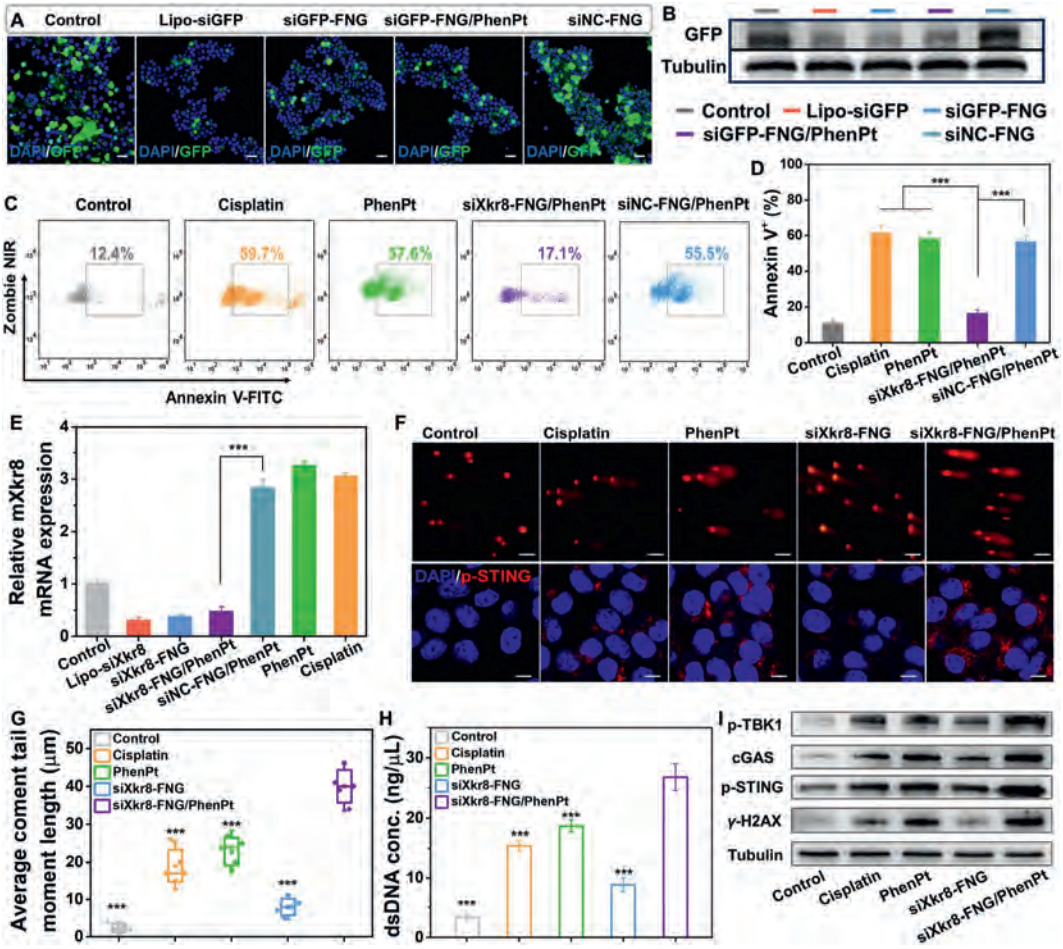

Figure 3 siRNA-mediated gene silencing. The expression of GFP was detected by CLSM (A) and (B) WB analysis (the scale bar represents 25 μm, DAPI (blue): $\lambda_{ex}/\lambda_{em}$ = 364 nm/454 nm, GFP (green): $\lambda_{ex}/\lambda_{em}$ = 488 nm/507 nm). (C) The FCM results and (D) data statistics reflect the proportions of Annexin V^+ in 4T1 cells (n = 3, mean ± SD, ***P < 0.005). (E) Relative *mXkr8* mRNA expression in 4T1 cells determined by RT-qPCR (n = 3, mean ± SD, ***P < 0.005). (F) Representative fluorescence images of comet assays to evaluate fragmented DNA levels in 4T1 cells (scale bars: 50 μm, PI (red): $\lambda_{ex}/\lambda_{em}$ = 535 nm/617 nm). CLSM of 4T1 cells treated with p-STING protein-specific antibody after various treatments (the scale bar represents 10 μm, DAPI (blue): $\lambda_{ex}/\lambda_{em}$ = 364 nm/454 nm, Alexa Fluor 647 (red): $\lambda_{ex}/\lambda_{em}$ = 651 nm/667 nm). (G) Calculated lengths of the comet tails in (F) (***P < 0.005 *vs*. siXkr8-FNG/PhenPt). (H) Quantification of dsDNA in the supernatant of the 4T1 cells (n = 3, mean ± SD, ***P < 0.005 *vs*. siXkr8-FNG/PhenPt). (I) The WB analysis of proteins extracted from 4T1 cells treated with different treatments.

based drugs. Exposure of PS was measured by Annexin V-FITC staining and FCM. As shown in Fig. 3C and D, the positive rate of Annexin V was significantly increased in the cancer cells treated with cisplatin and PhenPt, which were 59.7% and 57.6%, respectively. The positive rate of Annexin V in siNC-FNG/PhenPt group was not significantly decreased, while the positive rate in cancer cells treated with siXkr8-FNG/PhenPt was significantly decreased to only 17.1%. In addition, Real-time quantitative polymerase chain reaction (RT-qPCR) was used to detect the silencing of endogenous genes by siXkr8-FNG/PhenPt. The results in Fig. 3E showed that treatment with cisplatin and PhenPt resulted in a significant upregulation of *Xkr8* mRNA, whereas positive control Lipo-siXkr8 and both siXkr8-FNG and siXkr8-FNG/PhenPt containing siXkr8 effectively inhibited *Xkr8* mRNA expression in 4T1 cells. Notably, siNC-FNG/PhenPt containing scrambled siRNA presented a similar effect to platinum-based drugs alone and did not significantly reduce *Xkr8* mRNA expression. This again demonstrated that target gene silencing is a sequence-specific RNAi process and that siXkr8-FNG significantly reduced platinum (PhenPt)-induced *Xkr8* mRNA upregulation. The construction of FNG increased the protective barrier for siRNA and reduced its exposure. siXkr8-FNG was enriched at the tumor site and efficiently taken up. Subsequently, the carrier shell (FNA nanogel) disintegrated in the intracellular acidic environment and in the presence of RNase to release the "core" siXkr8. The multi-dimensional strategy of tumor enrichment and release control significantly reduced the off-target effects of FNG loaded siRNA. Thus, siXkr8-FNG/PhenPt effectively blocked the expression of Xkr8 and reduced the exposure of PS on the outer surface of cancer cells.

3.4. SiXkr8-FNG/PhenPt activates the STING pathway

Current studies have also proved that PhenPt can activate the cGAS−STING pathway and achieve chemo-immune synergy for tumor treatment[12,13]. Therefore, we further investigated the effect of PhenPt-loaded siXkr8-FNG on STING pathway activation. The DNA damage in siXkr8-FNG/PhenPt-treated cells was explored by single-cell gel electrophoresis using the comet assay (Fig. 3F and G). The nuclei of cells in the PBS group were spherical, while most cells treated with siXkr8-FNG/PhenPt had a "comet" tail, which is formed by the migration of damaged DNA (comet tail) from nucleoid (comet head), indicating that siXkr8-FNG/PhenPt induced severe DNA damage. Subsequently, the release of dsDNA was evaluated to the supernatant of the 4T1 cells. As shown in Fig. 3H, there was a significant increase in the concentration of dsDNA in the treated cells in each group compared to the dsDNA concentration in the control cells. In contrast, the concentration of dsDNA in 4T1 cells after siXkr8-FNG/PhenPt treatment was 7.7-fold higher than that in control group, respectively. This further confirms the DNA damage and dsDNA release induced by siXkr8-FNG/PhenPt effectively. The results of Fig. 3I and Fig. S7B showed that siXkr8-FNG/PhenPt could increase the expression level of γ-H2AX, suggesting that it could induce DNA double-strand breaks. Phosphorylated STING (p-STING), cGAS and phosphorylated TBK-1 (p-TBK1) have been previously identified as key components in the activation of the cGAS−STING pathway[9,33]. Excitingly, WB analysis (Fig. 3G and H) revealed enhanced expression levels of the above proteins, with siXkr8-FNG/PhenPt having the strongest expression level, and the CLSM images (Fig. 3F) supported the above results. In addition, supernatants of 4T1 cells treated with each preparation were used to examine the dendritic cells (DCs) activation capability of 4T1-tumor-cell-derived dsDNA. Treatment with siXkr8-FNG/PhenPt significantly increased the expression of CD80 and CD86 compared with controls. The proportion of $CD80^+CD86^+$ in group siXkr8-FNG/PhenPt was 1.38-fold, 1.22-fold, and 1.7-fold higher than that in groups Cisplatin, PhenPt, and siXkr8-FNG, respectively (Supporting Information Fig. S8), further confirming that siXkr8-FNG/PhenPt induced dsDNA release and DCs maturation. Overall, siXkr8-FNG/PhenPt could achieve target gene silencing, blocking Xkr8 expression, preventing PS ectopia, while loading PhenPt, inducing DNA damage, and synergizing with DNA nanostructures to co-activate the cGAS−STING pathway, thus presenting a multimodal chemo-immunological nanoformulation.

3.5. In vivo anticancer effect of siXkr8-FNG/PhenPt

SiXkr8-FNG/PhenPt showed excellent performance in inhibiting tumor cell proliferation *in vitro,* and schematic diagram of the timeline is shown in Fig. 4A. The *in vivo* anticancer effect was evaluated in a 4T1-bearing mouse model. First, the *in vivo* biodistribution of siXkr8-FNG/PhenPt was traced by an IVIS imaging system. Both free Cy5 and siXkr8-FNG/PhenPt (Cy5-modified siXkr8-FNG) showed strong fluorescence in mice (Fig. 4B). Notably, siXkr8-FNG/PhenPt gradually gathered at the tumor site, and still showed bright fluorescence 12 h after intravenous administration, indicating that siXkr8-FNG/PhenPt accumulated more in the tumor. The results of *ex vivo* imaging and fluorescence semi-quantitative statistics (Fig. 4C) were consistent with the above results. In addition, in order to visually demonstrate the ability of siXkr8-FNG/PhenPt accumulation at the tumor location, the platinum content in major organs and tumors of 4T1 tumor-bearing mice was also determined by ICP-MS. Encouragingly, the platinum content in the tumor tissues was significantly higher than that in the other five organs (Fig. 4D). These results indicated that the nanomaterials have the desired tumor-targeting properties and could achieve effective accumulation at the tumor site, which laid the foundation for subsequent *in vivo* tumor suppression.

Encouraged by the excellent antitumor effect *in vitro* and tumor enrichment ability of siXkr8-FNG/PhenPt, five treatments including saline, free PhenPt, siXkr8-FNG, siXkr8-FNG/PhenPt and siNC-FNG/PhenPt (FNG with scrambled siRNA) were administered intravenously to 4T1-bearing mice, respectively. Fig. 4E and F results show the body weight and tumor growth of the mice after treatment. Saline did not have any inhibitory effect on the tumor and the tumor volume increased rapidly, while the remaining groups showed some degree of antitumor effect. Notably, although PhenPt had a certain degree of tumor inhibition, with a tumor suppression rate of about 56.96% (Fig. 4G), the mice showed a significant decrease in body weight after treatment. In contrast, the siXkr8-FNG and PhenPt-DNA complex groups did not cause any decrease in body weight of the mice, and the H&E section staining (Supporting Information Fig. S9) of the five organs did not show any obvious tissue or organ toxicity. Relevant blood routine indexes and serum biochemistry results, such as white blood cell (WBC), red blood cell (RBC), hemoglobin (HGB), blood urea nitrogen (BUN), alanine aminotransferase (ALT), alkaline phosphatase (ALP), etc. (Supporting Information Fig. S10), also showed that siXkr8-FNG/PhenPt had good blood compatibility. These results demonstrated that the PhenPt-DNA complexes greatly improved the biosafety of the free cationic form of PhenPt and broadened its application *in vivo*. Among

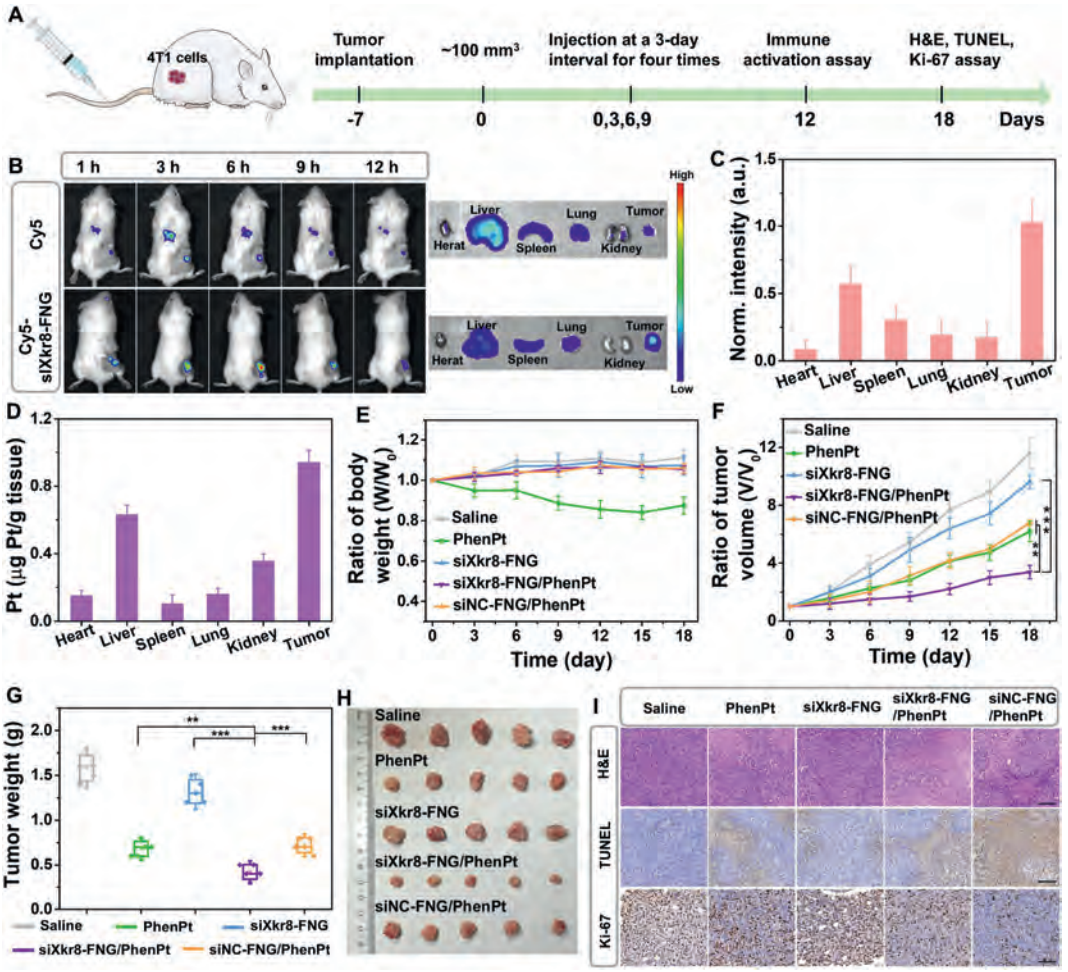

Figure 4 *In vivo* anticancer effect of siXkr8-FNG/PhenPt. (A) Schematic illustration of the timeline. (B) Biodistribution in 4T1-bearing mouse model after injection of free Cy5 and siXkr8-FNG/PhenPt (Cy5 (red): $\lambda_{ex}/\lambda_{em}$ = 650 nm/670 nm). (C) The semi-quantitative analysis of fluorescence intensity. (D) The Pt content in different organs and tumor samples after injection of siXkr8-FNG/PhenPt. The body weight (E) and tumor growth inhibition (F) curves after various treatments (n = 5, mean ± SD, $^{**}P < 0.01$, $^{***}P < 0.005$). (G) The tumor weight after different treatments (n = 5, mean ± SD, $^{**}P < 0.01$, $^{***}P < 0.005$). (H) Photographs of the tumors after various treatments. (I) H&E, TUNEL and Ki-67 staining images of tumor tissues after various treatments (the scale bar represents 100 μm).

them, DNA matrix composite siXkr8-FNG/PhenPt combined with siXkr8 and PhenPt demonstrated minimal tumor volume and tumor weight after treatment (Fig. 4F−H), with a tumor suppression rate as high as 73.42%, showing the best therapeutic effect. The H&E, TUNEL and Ki-67 staining images (Fig. 4I) of the tumor tissues showed extensive nuclear shrinkage and DNA damage in the tumor tissues after siXkr8-FNG/PhenPt treatment, indicating that siXkr8-FNG/PhenPt significantly inhibited the proliferation of tumor cells and tumors presented a high rate of apoptosis. The above results collectively indicate that siXkr8-FNG/PhenPt has significant biosafety and potential anticancer activity *in vivo*.

3.6. Activation of immune responses by siXkr8-FNG/PhenPt in vivo

Previous studies have reported that both PhenPt and FNA activate the STING pathway and activate immunity[12,30]. Therefore, immunotherapy analysis in 4T1-tumor-bearing mice after treatment was performed to explore the activation of immune responses and antitumor mechanism. It is well known that PS exposure on the outer surface of cancer cells induced by chemotherapy is an important signal of immunosuppression[16]. Firstly, the positive proportion of Annexin V in tumor tissues of tumor-bearing mice in each group after administration was determined by FCM. As shown in Fig. 5A and B, treatment with PhenPt and siNC-FNG/PhenPt (FNG with scrambled siRNA) resulted in a significant increase in the level of phosphatidylserine on the cell surface, approximately 25.0% and 26.6%, respectively, while the positive rate of Annexin V in tumor tissue treated with siXkr8-FNG/PhenPt decreased significantly, only 14.7%. The results were consistent with the effect of gene silencing *in vitro*, indicating that siXkr8-FNG/PhenPt could effectively block the expression of Xkr8, reduce the exposure of PS, and provide a boost to alleviate immunosuppression.

DCs are the most important antigen-presenting cells responsible for the activation and regulation of innate and adaptive immunity[34]. Immature DCs phagocytose exogenous substances such as antigens, which are then presented by mature DCs to the major histocompatibility complex (MHC), which is recognized by T cell receptors to activate T cells, triggering an immune response[34,35]. Therefore, the promotion of DCs maturation by different types of

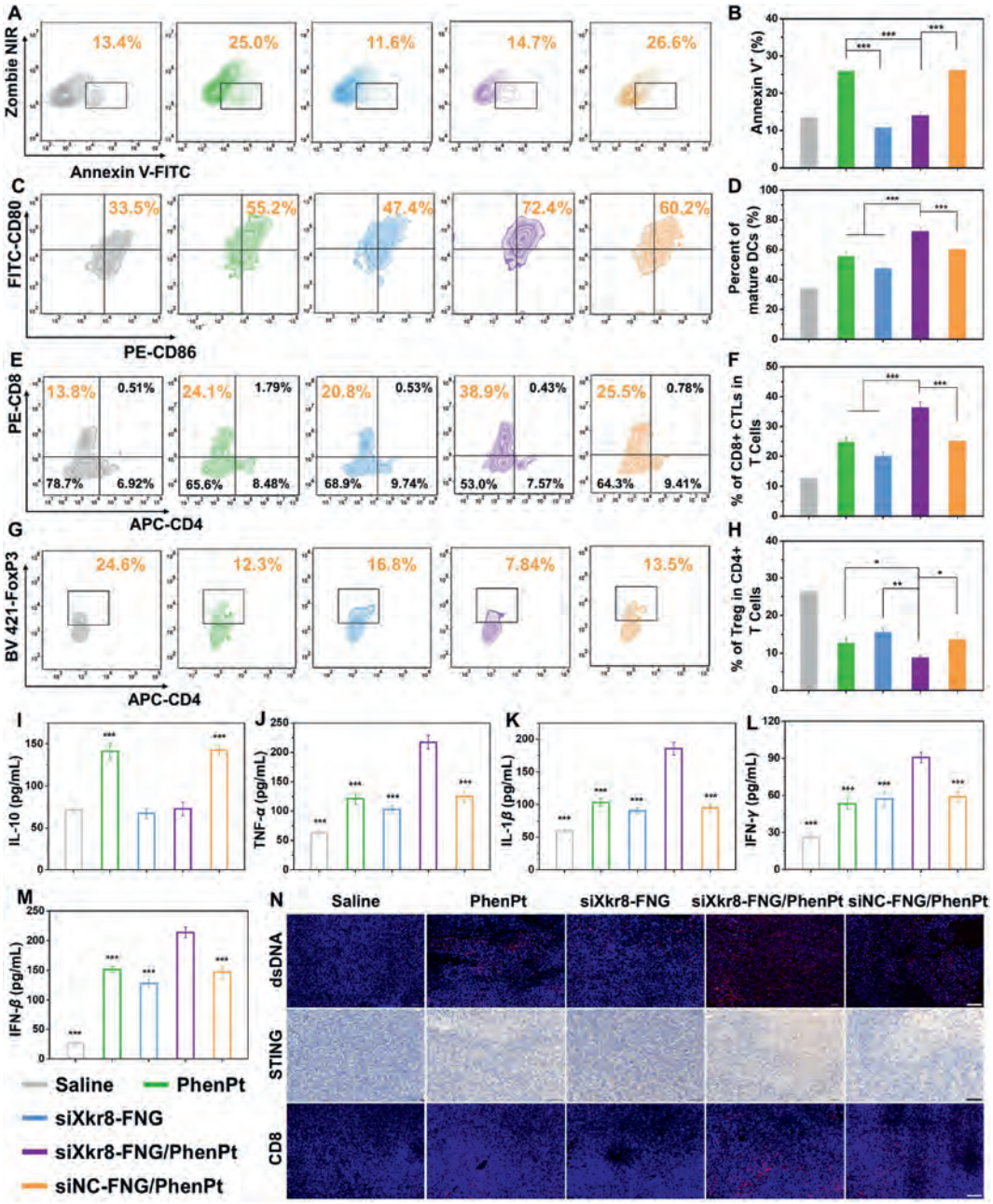

Figure 5 Activation of immune responses by siXkr8-FNG/PhenPt *in vivo*. (A) FCM and (B) statistical analysis of Annexin V^+ tumor cells after different formulations. (C) FCM and (D) statistical analysis of mature DCs *in vivo*. (E, G) FCM of tumors after staining with CD3, CD8, CD4 and FoxP3. (F) Proportions of $CD8^+$ CTLs in T cells. (H) Proportions of Treg in $CD4^+$ T cells. $n = 3$, $^*P < 0.05$, $^{**}P < 0.01$, $^{***}P < 0.005$. (I–M) The levels of IL-10, TNF-α, IL-1β, IFN-γ and IL-1β ($n = 3$, $^*P < 0.05$, $^{**}P < 0.01$, $^{***}P < 0.005$ *vs.* siXkr8-FNG/PhenPt). (N) Immunohistochemical/fluorescence images of dsDNA (scale bar: 100 μm, DAPI (blue): $\lambda_{ex}/\lambda_{em}$ = 364 nm/454 nm, Alexa Fluor 647 (red): $\lambda_{ex}/\lambda_{em}$ = 651 nm/667 nm), STING and CD8 (scale bar: 50 μm, DAPI (blue): $\lambda_{ex}/\lambda_{em}$ = 364 nm/454 nm, Alexa Fluor 647 (red): $\lambda_{ex}/\lambda_{em}$ = 651 nm/667 nm).

nanoparticles was first investigated. As shown in Fig. 5C and D, all nanoparticles promoted DCs maturation compared with saline. As expected, the percentage of mature DCs ($CD80^+CD86^+$) induced by siXkr8-FNG/PhenPt treatment was about 76.8%, which was significantly higher than that of the PhenPt and the siXkr8-FNG group, indicating that siXkr8-FNG/PhenPt could effectively promote the maturation of DCs. Maturation of DCs contributes to T cell activation, and next, activation of $CD8^+$ cytotoxic T lymphocytes ($CD8^+$ CTLs) in tumor tissues was determined. Fig. 5E and F results show that the activation levels of $CD8^+$ CTLs was consistent with the trend of DCs maturation, and the level of $CD8^+$ CTLs cells induced by siXkr8-FNG/PhenPt was the highest, about 34.9%, which was significantly higher than that of other treatment groups. Immune-suppressive regulatory T cells (Treg) are normally enriched in tumors to protect tumor cells from the immune system. Equally excitingly, treatment with siXkr8-FNG/PhenPt also significantly reduced the proportion of Treg cells (Fig. 5G and H), demonstrating the potential of this system to reverse the immunosuppressive microenvironment. Overall, siXkr8-FNG/PhenPt could reduce the exposure of PS, promote

DCs maturation and predict the proliferation and activation of T cells, and exhibit the potential to remodel the immunosuppressive microenvironment.

The engagement between PS-exposed tumor cells and macrophages has been reported to induce the secretion of interleukin-10 (IL-10), which can polarize macrophages to an immunosuppressive phenotype[36]. And the activation of the cGAS−STING pathway can mediate the secretion of interferon and other pro-inflammatory factors, thereby remodeling the immunosuppressive microenvironment and ultimately enhancing antitumor immunity. Therefore, the secretion levels of IL-10 and other relevant cytokines were detected using enzyme-linked immunosorbent assay (ELISA) to further validate the immune response. The results (Fig. 5I) demonstrate that IL-10 levels were increased in mice treated with PhentPt and siNC-FNG/PhenPt, whereas IL-10 secretion was significantly decreased after siXkr8-FNG/PhenPt treatment. In addition, siXkr8-FNG/PhenPt treatment significantly promoted the secretion of tumor necrosis factor (TNF-α), interleukin-1β (IL-1β), interferon-γ (IFN-γ) and interferons (IFN-β) indicating the strongest immune response (Fig. 5J−M), which was consistent with the results of the immune response analysis described above. The immunohistochemical/fluorescence images (Fig. 5N) demonstrated a large number of dsDNA, STING and CD8-positive spots in the tumor sections after siXkr8-FNG/PhenPt treatment, further suggesting infiltration of T cells and overexpression of STING protein in the tumor tissue. A series of immune activation results showed that siXkr8-FNG/PhenPt could induce T cell activation through activating the STING pathway, eliciting immune response, and reprogramming the inhibitory immune microenvironment, promoting the secretion of related cytokine, and further enhance the antitumor immune effect to achieve efficient tumor treatment.

3.7. Anticancer effect of siXkr8-FNG/PhenPt in metastatic animal models

Lung metastasis is a common distal metastasis site of breast cancer, and it is also one of the important causes of death of breast cancer[37,38]. First, a mouse lung metastasis model was established (Fig. 6A) to explore the inhibitory effect of siXkr8-FNG/PhenPt

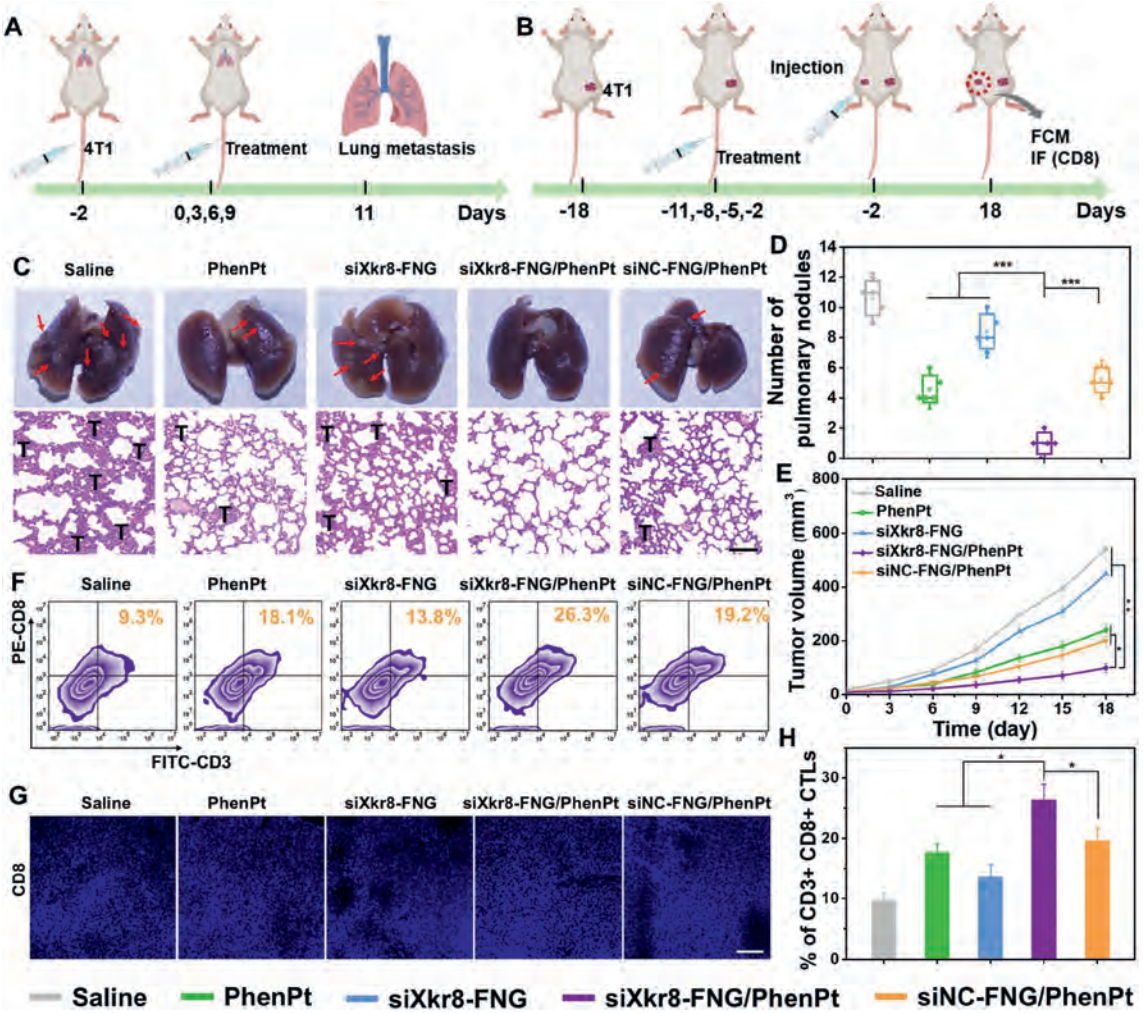

Figure 6 Immune response evaluation *in vivo*. Schematic illustration of (A) lung metastasis model and (B) distant tumor model. (C) Representative lung images and images of H&E (T indicates the lung metastasis, scale bar: 100 μm). (D) Statistics on the number of pulmonary nodules ($n = 5$, $^{*}P < 0.05$, $^{**}P < 0.01$, $^{***}P < 0.005$). (E) The volume change of the metastatic tumors after different formulations ($n = 5$, $^{*}P < 0.05$, $^{**}P < 0.01$). (F) FCM analysis and (H) the percentage of $CD3^{+}CD8^{+}$ T cells populations in the metastatic tumor ($n = 3$, $^{*}P < 0.05$, $^{**}P < 0.01$). (G) Immunofluorescence of CD8 in the metastatic tumors of mice with various treatments (scale bar: 100 μm, DAPI (blue): $\lambda_{ex}/\lambda_{em} = 364$ nm/454 nm, Alexa Fluor 647 (red): $\lambda_{ex}/\lambda_{em} = 651$ nm/667 nm).

on breast cancer lung metastasis. As shown in Fig. 6C and D, representative whole-lung images and H&E staining of mice showed the number and size of metastatic nodules in lung tumors were significantly reduced after siXkr8-FNG/PhenPt treatment compared with mice treated with saline and other drugs. These results suggested that siXkr8-FNG/PhenPt could inhibit tumor metastasis to the lung.

Furthermore, to investigate whether the triggered immune response could inhibit the growth of metastatic tumors, artificial mock metastatic tumors were constructed (Fig. 6B). The volume change and mass of the metastatic tumors, and the weight change of the mice were shown in Fig. 6E and Supporting Information Fig. S11. Except for free PhenPt, the other drug preparation groups did not cause weight loss in mice, suggesting that the vector has good biological safety. As we expected, the mass of metastatic tumors after treatment with siXkr8-FNG/PhenPt was the lowest, proving that siXkr8-FNG/PhenPt has great therapeutic potential for metastatic tumors. Encouragingly, elevated levels of cytotoxic T cells ($CD3^+$ $CD8^+$) were observed (Fig. 6F and H), and immunohistochemical images (Fig. 6G) also revealed the increased expression of $CD8^+$ T cells, indicating potent immunogenic therapeutic effect against metastatic tumor. Together, these results indicate that treatment with siXkr8-FNG/PhenPt could generate a strong immune response and has a good anticancer effect on metastatic tumors.

4. Conclusions

Pt-based antineoplastic drugs have serious side effects and lead to tumor immunosuppression in clinical applications. Reduction of extracellular surface phosphatidylserine exposure by siXkr8 is an effective way to reduce tumor immunosuppression. Here, we report the construction and mechanistic studies of novel siRNA-mediated PhenPt-loaded FNA nanogels (siXkr8-FNG/PhenPt) for enhanced chemo-immunotherapy. SiXkr8-FNG/PhenPt not only deliver PhenPt to reduce its toxicity for effective chemotherapy; but also activate the cGAS−STING pathway to stimulate the immune response. Most importantly, siXkr8-FNG/PhenPt could effectively block the expression of Xkr8 and reduce the exposure of PS on the cancer cells surface, while promoting DCs maturation and immunogenicity, synergistically enhancing the effective immune stimulation of TIL, triggering a stronger antitumor immunotherapy, and significantly inhibiting tumor growth and metastasis. Due to its precise geometry, programmability and biocompatibility, FNA has become a research hotspot for novel drug delivery systems. However, due to the small particle size in the blood circulation, it is easy to be eliminated, and faces the risk of enzymatic degradation, etc., optimizing the design strategy, reducing costs, and accumulating *in vivo* safety data will be the focus of future research. The construction of FNA nanogel expands the structural design and application of FNA, and provides a new strategy for delivering siRNA. While greatly improving the efficacy of Pt-based drugs and reducing immunosuppression, it represents a promising strategy to improve cancer chemoimmunotherapy.

Acknowledgments

This research was financially supported by the Natural Science Foundation of Shandong province (ZR2023QH204 and ZR2024ME024, China).

Author contributions

Jianqin Yan: data curation, investigation, methodology, formal analysis, conceptualization, supervision, writing-original draft. Zijian Zhao: formal analysis, investigation, methodology. Dengshuai Wei: writing-original draft, methodology. Huapeng Zheng: formal analysis, methodology. Bin He: writing-original draft. Yong Sun: supervision, resources, writing-original draft.

Conflicts of interest

The authors declare no conflict of interest.

Appendix A. Supporting information

Supporting information to this article can be found online at https://doi.org/10.1016/j.apsb.2025.07.027.

References

1. Xu ZH, Wang YH, Zhang L, Huang L. Nanoparticle-delivered transforming growth factor-β siRNA enhances vaccination against advanced melanoma by modifying tumor microenvironment. *ACS Nano* 2014;**8**:3636−45.
2. Chen YN, Zhou QQ, Jia ZF, Cheng N, Zhang S, Chen WD, et al. Enhancing cancer immunotherapy: nanotechnology-mediated immunotherapy overcoming immunosuppression. *Acta Pharm Sin B* 2024;**14**:3834−54.
3. Joyce JA, Fearon DT. T cell exclusion, immune privilege, and the tumor microenvironment. *Science* 2015;**348**:74−80.
4. Galon J, Bruni D. Approaches to treat immune hot, altered and cold tumours with combination immunotherapies. *Nat Rev Drug Discov* 2019;**18**:197−218.
5. Tang HD, Wang Y, Chlewicki LK, Zhang Y, Guo JY, Liang W, et al. Facilitating T cell infiltration in tumor microenvironment overcomes resistance to PD-L1 blockade. *Cancer Cell* 2016;**30**:500.
6. Binnewies M, Roberts EW, Kersten K, Chan V, Fearon DF, Merad M, et al. Understanding the tumor immune microenvironment (TIME) for effective therapy. *Nat Med* 2018;**24**:541−50.
7. Du JM, Qian MJ, Yuan T, Chen RH, He QJ, Yang B, et al. cGAS and cancer therapy: a double-edged sword. *Acta Pharmacol Sin* 2022;**43**:2202−11.
8. Vargas TR, Benoit-Lizon I, Apetoh L. Rationale for stimulator of interferon genes-targeted cancer immunotherapy. *Eur J Cancer* 2017;**75**:86−97.
9. Shae D, Becker KW, Christov P, Yun DS, Lytton-Jean AKR, Sevimli S, et al. Endosomolytic polymersomes increase the activity of cyclic dinucleotide STING agonists to enhance cancer immunotherapy. *Nat Nanotechnol* 2019;**14**:269−78.
10. Kellinger MW, Park GY, Chong J, Lippard SJ, Wang D. Effect of a monofunctional phenanthriplatin-DNA adduct on RNA polymerase II transcriptional fidelity and translesion synthesis. *J Am Chem Soc* 2013;**135**:13054−61.
11. Johnstone TC, Alexander SM, Lin W, Lippard SJ. Effects of monofunctional platinum agents on bacterial growth: a retrospective study. *J Am Chem Soc* 2014;**136**:116−8.
12. Zhang LP, Shang K, Li XM, Shen MF, Lu S, Tang DS, et al. Reduction sensitive polymers delivering cationic platinum drugs as STING agonists for enhanced chemo-immunotherapy. *Adv Funct Mater* 2022;**32**:2204589.
13. Chen H, Wang YS, Liu YL, Tang L, Mu QC, Yin XY, et al. Delivery of cationic platinum prodrugs *via* reduction sensitive polymer for improved chemotherapy. *Small* 2021;**17**:e2101804.
14. Wang WH, Wu SX, Cen ZP, Zhang YX, Chen Y, Huang YX, et al. Mobilizing phospholipids on tumor plasma membrane implicates

phosphatidylserine externalization blockade for cancer immunotherapy. *Cell Rep* 2022;**41**:111582.
15. Chen YA, Huang YX, Li QZ, Luo ZY, Zhang ZQ, Huang HZ, et al. Targeting Xkr8 *via* nanoparticle-mediated *in situ* co-delivery of siRNA and chemotherapy drugs for cancer immunochemotherapy. *Nat Nanotechnol* 2023;**18**:193−204.
16. Birge RB, Boeltz S, Kumar S, Carlson J, Wanderley J, Calianese D, et al. Phosphatidylserine is a global immunosuppressive signal in efferocytosis, infectious disease, and cancer. *Cell Death Differ* 2016;**23**:962−78.
17. Li Z, Zhang L, Jiang K, Zhang Y, Liu Y, Hu G, et al. Biosafety assessment of delivery systems for clinical nucleic acid therapeutics. *Biosafety Health* 2022;**4**:105−17.
18. Kim T, Viard M, Afonin KA, Gupta K, Popov M, Salotti J, et al. Characterization of cationic bolaamphiphile vesicles for siRNA delivery into tumors and brain. *Mol Ther-Nucl Acids* 2020;**20**: 359−72.
19. Hu B, Zhong LP, Weng YH, Peng L, Huang YY, Zhao YX, et al. Therapeutic siRNA: state of the art. *Signal Transduct Targeted Ther* 2020;**5**:1210−34.
20. Ferrer JR, Sinegra AJ, Ivancic D, Yeap XY, Qiu LH, Wang JJ, et al. Structure-dependent biodistribution of liposomal spherical nucleic acids. *ACS Nano* 2020;**14**:1682−93.
21. Vasher MK, Yamankurt G, Mirkin CA. Hairpin-like siRNA-based spherical nucleic acids. *J Am Chem Soc* 2022;**144**:3174−81.
22. Yan JQ, Yu HL, Liu CL, Li B, Wei DS, He B, et al. Low-temperature photothermal-chemotherapy enhancing tumor immunotherapy by tetrahedral framework nucleic acids nanogels based drug delivery system. *Chem Eng J* 2024;**481**:148616.
23. Keller A, Linko V. Challenges and perspectives of DNA nanostructures in biomedicine. *Angew Chem-Int Edit* 2020;**59**:15818−33.
24. Xue H, Ding F, Zhang J, Guo YY, Gao XH, Feng J, et al. DNA tetrahedron-based nanogels for siRNA delivery and gene silencing. *Chem Commun* 2019;**55**:4222−5.
25. Yan JQ, Yu HL, Tang XW, Li FS, Li ZP, Liang Y, et al. Highly triple-effective synergy based on tetrahedral DNA nanostructure-induced tumor vaccines for cancer therapy. *Mater Des* 2023;**226**: 111584.
26. Yan JQ, Zhang N, Zhang ZZ, Zhu WW, Li B, Li L, et al. Redox-responsive polyethyleneimine/tetrahedron DNA/doxorubicin nanocomplexes for deep cell/tissue penetration to overcome multidrug resistance. *J Control Release* 2021;**329**:36−49.
27. Keller W, Crouch R. Degradation of DNA RNA hybrids by ribonuclease H and DNA polymerases of cellular and viral origin. *Proc Natl Acad Sci U S A* 1972;**69**:3360−4.
28. Almaqwashi AA, Zhou W, Naufer MN, Riddell IA, Yilmaz ÖH, Lippard SJ, et al. DNA intercalation facilitates efficient DNA-targeted covalent binding of phenanthriplatin. *J Am Chem Soc* 2019;**141**:1537−45.
29. Wang LN, Yu YJ, Wei DS, Zhang LP, Zhang XY, Zhang GX, et al. A Systematic strategy of combinational blow for overcoming cascade drug resistance *via* NIR-light-triggered hyperthermia. *Adv Mater* 2021;**33**:e2100599.
30. Liang SP, Li JY, Zou ZY, Mao M, Ming SQ, Lin F, et al. Tetrahedral DNA nanostructures synergize with MnO_2 to enhance antitumor immunity *via* promoting STING activation and M1 polarization. *Acta Pharm Sin B* 2022;**12**:2494−505.
31. Zhang LP, Wang YQ, Karges J, Tang DS, Zhang HC, Zou KX, et al. Tetrahedral DNA nanostructure with interferon stimulatory DNA delivers highly potent toxins and activates the cGAS−STING pathway for robust chemotherapy and immunotherapy. *Adv Mater* 2023;**35**:e2210267.
32. Zhang X, Xu XH, Li YC, Hu C, Zhang ZJ, Gu ZW. Virion-like membrane-breaking nanoparticles with tumor-activated cell-and-tissue dual-penetration conquer impermeable cancer. *Adv Mater* 2018;**30**: e1707240.
33. Sun XQ, Zhang Y, Li JQ, Park KS, Han K, Zhou XW, et al. Amplifying STING activation by cyclic dinucleotide-manganese particles for local and systemic cancer metalloimmunotherapy. *Nat Nanotechnol* 2021;**16**:1260−70.
34. Janeway CA, Bottomly K. Signals and signs for lymphocyte responses. *Cell* 1994;**76**:275−85.
35. Chen Q, Chen JW, Yang ZJ, Xu J, Xu LG, Liang C, et al. Nanoparticle-enhanced radiotherapy to trigger robust cancer immunotherapy. *Adv Mater* 2019;**31**:e1802228.
36. Qi L, Yu HQ, Zhang Y, Zhao DH, Lv P, Zhong Y, et al. IL-10 secreted by M2 macrophage promoted tumorigenesis through interaction with JAK2 in glioma. *Oncotarget* 2016;**7**:71673−85.
37. Geng WW, An JH, Dong K, Zhang HL, Zhang XY, Liu YC, et al. ZNF8 orchestrates with Smad3 to promote lung metastasis by recruiting SMYD3 in breast cancer. *Adv Sci (Weinh)* 2024;**11**: e2404904.
38. Zhao ZT, Fang L, Xiao P, Sun XS, Zhou L, Liu XC, et al. Walking dead tumor cells for targeted drug delivery against lung metastasis of triple-negative breast cancer. *Adv Mater* 2022;**34**:e2205462.